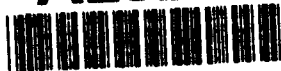


AD-A282 764



①

PL-TR-93-2267

Environmental Research Papers, No. 1136

**DETERMINATION OF THE AURORAL OVAL Q INDEX FROM
THE AIR WEATHER SERVICE K INDEX**

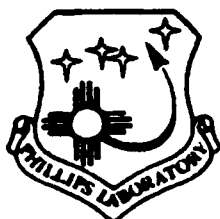
B. S. Dandekar

18 October 1993

DTIC
ELECTE
JUL 28 1994
S G D

APPROVED FOR PUBLIC RELEASE; DISTRIBUTION UNLIMITED

DTIC QUALITY INSPECTED 5



PHILLIPS LABORATORY
Directorate of Geophysics
AIR FORCE MATERIEL COMMAND
HANSCOM AIR FORCE BASE, MA 01731-3010

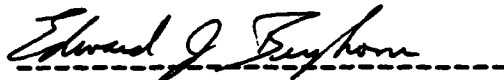
94-23824



3210

94 7 26 079

"This technical report has been reviewed and is approved for publication."



Maj Edward Berghorn, Chief
Ionospheric Application Branch



WILLIAM K. VICKERY, Director
Ionospheric Effects Division

This report has been reviewed by the ESC Public Affairs Office (PA) and is releasable to the National Technical Information Service (NTIS).

Qualified requestors may obtain additional copies from the Defense Technical Information Center (DTIC). All others should apply to the National Technical Information Service (NTIS).

If your address has changed, or if you wish to be removed from the mailing list, or if the addressee is no longer employed by your organization, please notify PL/TSI, 29 Randolph Road, Hanscom AFB, MA 01731-3010. This will assist us in maintaining a current mailing list.

Do not return copies of this report unless contractual obligations or notices on a specific document requires that it be returned.

REPORT DOCUMENTATION PAGE			Form Approved OMB No. 0704-0188	
Public reporting burden for this collection of information is estimated to average 1 hour per response, including the time for reviewing instructions, searching existing data sources, gathering and maintaining the data needed, and completing and reviewing the collection of information. Send comments regarding this burden estimate or any other aspect of this collection of information, including suggestions for reducing this burden, to Washington Headquarters Services, Directorate for Information Operations and Reports, 1215 Jefferson Davis Highway, Suite 1204, Arlington, VA 22202-4302, and to the Office of Management and Budget, Paperwork Reduction Project (0704-0188), Washington, DC 20503.				
1. AGENCY USE ONLY (Leave blank)		2. REPORT DATE 18 October 1993		3. REPORT TYPE AND DATES COVERED Scientific Interim
4. TITLE AND SUBTITLE Determination of the Auroral Oval Q Index from the Air Weather Service K Index			5. FUNDING NUMBERS PE 62101F Proj 4643 TA GH Work Unit 01	
6. AUTHOR(S) B. S. Dandekar				
7. PERFORMING ORGANIZATION NAME(S) AND ADDRESS(ES) Phillips Laboratory (GPIA) 29 Randolph Road Hanscom AFB MA 01731-3010			8. PERFORMING ORGANIZATION REPORT NUMBER PL-TR-93-2267 ERP., No. 1136	
9. SPONSORING/MONITORING AGENCY NAME(S) AND ADDRESS(ES)			10. SPONSORING/MONITORING AGENCY REPORT NUMBER	
11. SUPPLEMENTARY NOTES This report will be of interest to the Air Weather Service for prediction/specification of high latitude ionospheric models.				
12a. DISTRIBUTION/AVAILABILITY STATEMENT Approved for Public Release; Distribution Unlimited			12b. DISTRIBUTION CODE	
13. ABSTRACT (Maximum 200 words) The AWS determines the auroral oval diameter in real time as a function of the Kp index from the particle precipitation measured aboard Defense Meteorological Satellites (DMSP). For the 'Q' index needed to drive the auroral algorithm in the AWS polar ionospheric model, Hardy determined a relation between the Kp and the Q index. The analysis indicates that the auroral oval index 'Q' computed from the AWS-K is overestimated. A least-squared deviation circle is fitted to the data base used in the Hardy algorithm. Using a four-year data set of Kp and Q observations, a new relation between the planetary magnetic activity index Kp and Q is determined to rectify this overestimation of the Q index. The new relation is :Q=0.964 Kp-0.3 for Kp<2 + and Q=2.04 Kp-2.7 for Kp>2 +. The improved, more precise Q values obtained from this relation will improve prediction of the auroral oval phenomena that affect the performance of the real time operational systems.				
14. SUBJECT TERMS Magnetic activity index Kp, Auroral oval index, Magnetic activity index Q.			15. NUMBER OF PAGES 32	
			16. PRICE CODE	
17. SECURITY CLASSIFI- CATION OF REPORT UNCLASSIFIED	18. SECURITYCLASSIFI- CATION OF THIS PAGE UNCLASSIFIED	19. SECURITY CLASSIFI- CATION OF ABSTRACT UNCLASSIFIED	20. LIMITATION OF ABSTRACT SAR	

Contents

1. INTRODUCTION	1
2. BACKGROUND	2
3. ANALYSIS	14
4. CONCLUSIONS	23
REFERENCES	25

Accession For	
NTIS CRA&I	<input checked="" type="checkbox"/>
DTIC TAB	<input checked="" type="checkbox"/>
Unannounced	<input type="checkbox"/>
Justification	
By	
Distribution /	
Availability Codes	
Dist	Avail and/or Special
A-1	

Illustrations

1. Determination of the Q Index Using Hardy Algorithm (Equation 3)	5
2. Least Squared Deviation Circle Fit to Madden-Gussenhoven Data (Equation 6)	7
3. Comparison of Starkov Equations (2 and 7).	9
4. Comparison of Particle Precipitation Oval for $K_p=0$ With Starkov Oval for $Q=0$.	10
5. Comparison of Starkov Oval for $Q=9$ With Particle Precipitation Ovals for $K_p=2$ and 4.	11
6. Auroral Equatorward Boundaries Near Midnight for Electrons, DMSP Aurora, ASCA Aurora, and 6300 Å Photometric Observations.	13
7A. Cumulative Population of Detrended Q Index for Years 1965, 1969, 1971, and 1974.	15
7B. Cumulative Population of K_p Index for Years 1965, 1969, 1971, and 1974.	16
8. Relation Between the K_p and the Q Index From the Four-Year Data.	19
9. Comparison of Auroral K_p Index With the Planetary K_p Index From CRRES Data of July-December 1990.	20
10. Comparison of the AWS-K Index With the Planetary K_p Index.	21

Tables

1. Regression Coefficients of Auroral Equatorward Boundaries vs Kp (Madden-Gussenhoven Data 1990).	3
2. Parameters for the Starkov Q and Particle Precipitation Kp Ovals.	18
3. Kp-Q Relation From Observed Kp-Q Data.	18
4. Kp-Q Relation From Oval Parameters.	22

Acknowledgments

The author thanks Dr. J. A. Whalen for his suggestions and Mr. J. Buchau for his interest in the work.

Determination of the Auroral Oval Q Index from the Air Weather Service K Index

1. INTRODUCTION

Ionospheric models such as the ITS-78 (Barghausen et al¹, 1969) and/or IONCAP (Lloyd et al,² 1978) are unable to predict the ionospheric parameters accurately: the critical frequency, the height of the peak electron density, and the thickness of the layers, for the high latitude region affected by auroral enhancements, and for the midlatitude F layer trough, which is the region of ionospheric depletion. To overcome this deficiency, the Air Force Global Weather Central (AFGWC) developed the Polar Ionospheric model (see Millman et al³) by modifying the ITS-78 model for the auroral enhancement and for the F-layer trough, to support systems like Over the Horizon Backscatter (OTHB) radars operating in the mid and high latitude regions.

The input for the ITS78/IONCAP models are the Julian day, the universal time, and the sunspot number. The AWS uses the effective sunspot number SSNeff determined from the f_oF_2 observations from the AWS network of the Digital Ionospheric Sounding Systems (DISS) and other ionosondes. In addition to the SSNeff, the Polar Ionospheric Model needs the magnetic activity indices: the planetary index Kp and the auroral oval index Q, which control respectively the midlatitude trough and the auroral oval algorithms in the model. For generating the real time 'Kp' index (AWS-K) the AWS maintains a network of eight magnetometer stations covering the European and the American sectors (see Prochaska⁴ and Dandekar⁵). At present the auroral Q index is measured at a single station at Sodankyla, Finland. This Q index is not available in real time to the AWS.

Ideally the Q index should be measured at an auroral latitude on its magnetic midnight meridian. When the Q index is measured at a single station, the observed value is lower⁶ when the rotation of the earth moves the station away from the auroral oval. The AWS has no network similar to that for the 'Kp' (AWS-K) index, for measuring the Q index. Because the Q index is not

available in real time, Hardy⁷ (private communication) developed a scheme of using the DMSP-satellite based particle precipitation measurements. On the basis of the analysis of the DMSP data^{8,9} (Gussenhoven et al 1981, Gussenhoven et al 1983), the satellite measurements provide the instantaneous Kp index. Hardy⁷ (private communication) derived an algorithm to relate the Kp and Q indices by matching the Starkov Q=0 optical auroral oval¹⁰ with the Kp=0 particle precipitation oval. During the OTH-B tests we noticed that the Q index determined from the Hardy algorithm is high, especially for low Kp values. This report gives a correction for the problem.

The first section discusses the Hardy algorithm. The second section seeks other sources for determining a reliable relation between the Q and Kp indices. A relation more precise than the Hardy algorithm will provide improved predictions for the auroral oval phenomena. The auroral oval is one of the important clutter sources for the systems like the OTHB-ECRS and WCRS radars, for which their northern sector coverage of high latitude region is affected by the ionospheric irregularities associated with the auroral oval and the trough. The improved prediction of the auroral oval will help in relating the high latitude clutter more closely with the auroral oval morphology.

2. BACKGROUND

In the absence of the real time auroral oval Q index, the AWS uses real time particle precipitation boundaries observed by satellite (Defense Meteorological Satellite Program DMSP) borne sensors. These polar orbiting satellites provide a capability for determining the precipitation boundary every 110 minutes. Gussenhoven et al^{8,9} derived hourly empirical relations between the precipitation boundary and the planetary magnetic activity index Kp. By using these relations Kp can be determined from the DMSP particle precipitation data. For convenience the latest set of the coefficients for the straight line fits available from the Madden and Gussenhoven study¹¹ is reproduced in Table 1 (Table 3 from their report). The table presents the results of the least squared deviation straight line fits between the observed boundary 'L_T' and the corresponding Kp index for hourly intervals of the corrected magnetic local time (CGT). The first column gives the time interval T (in CGT) and the second column lists the number of observations. The next three columns provide the slope A_T, the intercept B_T (at Kp=0), and the correlation coefficient 'C' for the fit. The correlation coefficient provides the level of confidence for the empirical fit. The percent population closely following the fit is between C² and C. Thus with |C|=0.707, 50 percent to 71 percent (more than half) of the population of the data follows the fit. A look at the last column of Table 1 shows a lack of correlation (|C|<0.6) for the intervals of 2-4 and of 9-16 hours. When the correlation is significant, the observed boundary can be used for estimating the Kp index by using the equation,

$$L_T = A_T K_p + B_T \quad (1)$$

Table 1. Regression Coefficients of Auroral Equatorward Boundaries vs Kp
(Madden-Gussenhoven Data 1990)

REGRESSION COEFFICIENTS OF AURORAL EQUATORWARD BOUNDARIES VS KP ALL BOUNDARIES, 1983-1990				
Magnetic Local Time	Number of. Boundaries	Intercept A_T	Slope B_T	Correlation Coefficient
00-01	2349	67.57	-1.62	-0.73
01-02	43	68.31	-1.39	-0.66
02-03	41	68.92	+0.03	+0.03
03-04	2741	67.07	-1.50	-0.56
04-05	12900	66.56	-1.82	-0.76
05-06	20682	67.28	-1.79	-0.78
06-07	16186	68.10	-1.83	-0.74
07-08	13369	68.17	-1.65	-0.68
08-09	17422	68.98	-1.58	-0.67
09-10	17873	69.13	-1.24	-0.56
10-11	6565	68.99	-1.00	-0.46
11-12	2218	68.54	-0.62	-0.30
12-13	1056	68.90	-0.34	-0.16
13-14	1296	70.76	-0.37	-0.18
14-15	1564	71.48	-0.63	-0.29
15-16	1785	72.73	-1.12	-0.50
16-17	3332	73.22	-1.46	-0.71
17-18	8193	72.20	-1.48	-0.74
18-19	19946	71.64	-1.64	-0.80
19-20	17347	71.09	-1.85	-0.82
20-21	17539	69.71	-1.66	-0.78
21-22	14175	69.25	-2.07	-0.84
22-23	16234	67.89	-1.88	-0.83
23-24	11205	67.18	-1.75	-0.81

where L_T is the observed boundary in CG latitude at given CGT T,

A_T is the slope of the fit for time T,

B_T is the intercept of the fit for time T, and

K_p is the level of magnetic activity at time T.

The intercept B_T is related to the radius of the auroral oval for $K_p=0$, and the slope A_T is the increase in the radius of the auroral oval for each unit increase in K_p .

Feldstein and Starkov¹² determined the auroral oval boundary from All Sky Camera (ASCA) observations, and related it to the oval index Q measured on the magnetic midnight meridian. We will refer to these as Starkov optical auroral ovals. In the nightside the particle precipitation boundary is practically coincident with the optical auroral oval boundary. Therefore Hardy⁷ matched the midnight boundary of the DMSP ($K_p=0$) particle precipitation with the Starkov ($Q=0$) optical auroral ovals for determining the K_p - Q relation. The Starkov optical auroral oval boundary¹⁰ is given by

$$\lambda_T = 90 - [(18 + 0.9Q + 5.1 \cos (15T-12))] \text{ for } Q \neq 0. \quad (2)$$

The resulting empirical relation derived by Hardy is given by

$$Q = 2K_p - 0.35 \quad (3)$$

In his report Hardy (private communication) notes that the midnight precipitation and optical auroral boundaries match, but the difference in the respective boundaries is successively larger as one moves away from the midnight sector to the noon sector. He reports that at $K_p=0$ the noon latitude of the Starkov optical auroral oval is 7.8° poleward from the particle precipitation oval, and for $K_p=3$ this latitude difference is 5° .

Figure 1 shows the plot of K_p - Q data obtained for 52 days (381 observations) during the tests of the ECRS and the WCRS radars. About 76 percent of the observations cluster around the line given by Eq. (3). Our inquiry to the AWS showed that when satellite data are absent, the ground based K_p (AWS-K) data are put into the Hardy Eq. (3) to determine the Q index. In Figure 1 these ground based discrete data levels lie right on the straight line given by Eq. (3) and produce the clusters. In this small data set, the nonclustered data show that less than 24 percent of the observations are satellite based. We feel that in Figure 1, the computed Q index is overestimated, especially for $K_p=1$ and 2 ($Q=1.65$ and 3.65 respectively), because experience shows that the $Q=3$ condition is approximately equal to that of $K_p=3$.

Not only is the point $K_p=3$, $Q=3$ below any of the lines; it is well below the average of the satellite data. However, the time of the satellite reading (in CGT) is not available. Without this time information, the movement of the auroral precipitation oval with respect to the optical oval

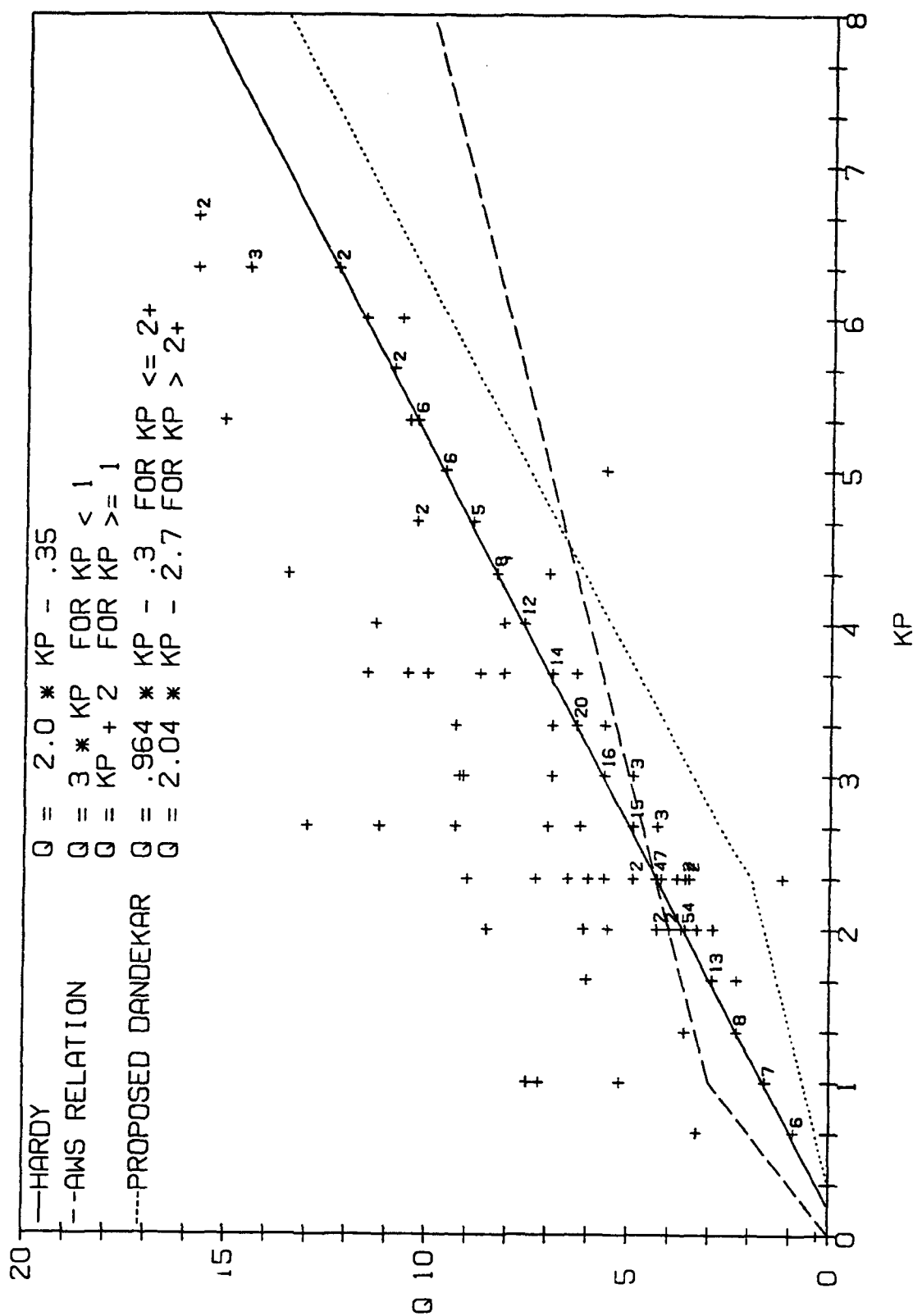


Figure 1. Determination of the Q Index Using Hardy Algorithm (Equation 3)

must remain unknown. In addition, the sample of satellite data is not large enough to be reliable statistically. These limitations motivated a search for a relationship that would reflect what we do know about the Kp-Q relationship, including the fact that Q=3 for Kp=3.

In the following we will compare the Starkov Q (optical) and the Kp particle precipitation ovals, to study the systematic differences between the Q and Kp auroral ovals for the determination of a more appropriate Kp-Q relation. Hardy used the hourly equations from Table 1 for determining the Kp index. In this study, two least squared deviation empirical circles were fitted, one to A_T and the other to B_T . For this purpose only the A_T - B_T values with $|C| \geq 0.6$ from Table 1 were used. The equation derived for the colatitude of the intercept is

$$B'_T = 90 - B_T = 20.27 + 3.37 \cos(15T - 41.8) \quad (4)$$

and the equation for the slope is

$$A_T = 1.69 + 0.24 \cos(15T - 13.8) \quad (5)$$

In each of the above equations the first term on the RHS gives the radius of the circle, the constant multiplier of the cosine term provides the offset (in latitude from the CG pole) of the circle from the center, and the number in the bracket of the cosine term presents the angular deviation (hour*15) from the midnight meridian. Combining the two equations provides an empirical fit between the observed boundary and the Kp index for the particle precipitation ovals. Substituting Eqs. (4) and (5) in Eq. (1) we get

$$\lambda_T = 90 - (20.27 + 3.37 \cos(15T - 42) + Kp \{ -[1.69 + 0.24 \cos(15T - 14)] \}) \quad (6)$$

This single equation (6) can be used in place of 16 T (time) sets of Eq. (1) from Table 1.

The comparison of Eqs. (2) and (6) is summarized in Table 2. The table shows that the radius of the Kp=0 particle precipitation oval is 0.6° larger than that of the Q=0 optical auroral oval. The center of the Q optical auroral oval is 1.7° equatorward of that of the Kp auroral oval. The radius of the Kp auroral oval increases at 1.7° per unit Kp, whereas the radius of the optical auroral oval increases at 0.9° per unit Q. Thus, the respective auroral ovals have different starting locations and different rates of expansion with the increase in the level of magnetic activity. Therefore forcing a match between the two auroral ovals at the midnight meridian results in increasing differences, with increasing level of magnetic activity, in their locations at meridians away from the (CG) midnight.

The data from Table 1 and the empirical circle fit from Eq. (6) are shown in Figure 2. The data points with $|C| < 0.6$ are not used in the study and are not plotted in Figure 2. The cause of the

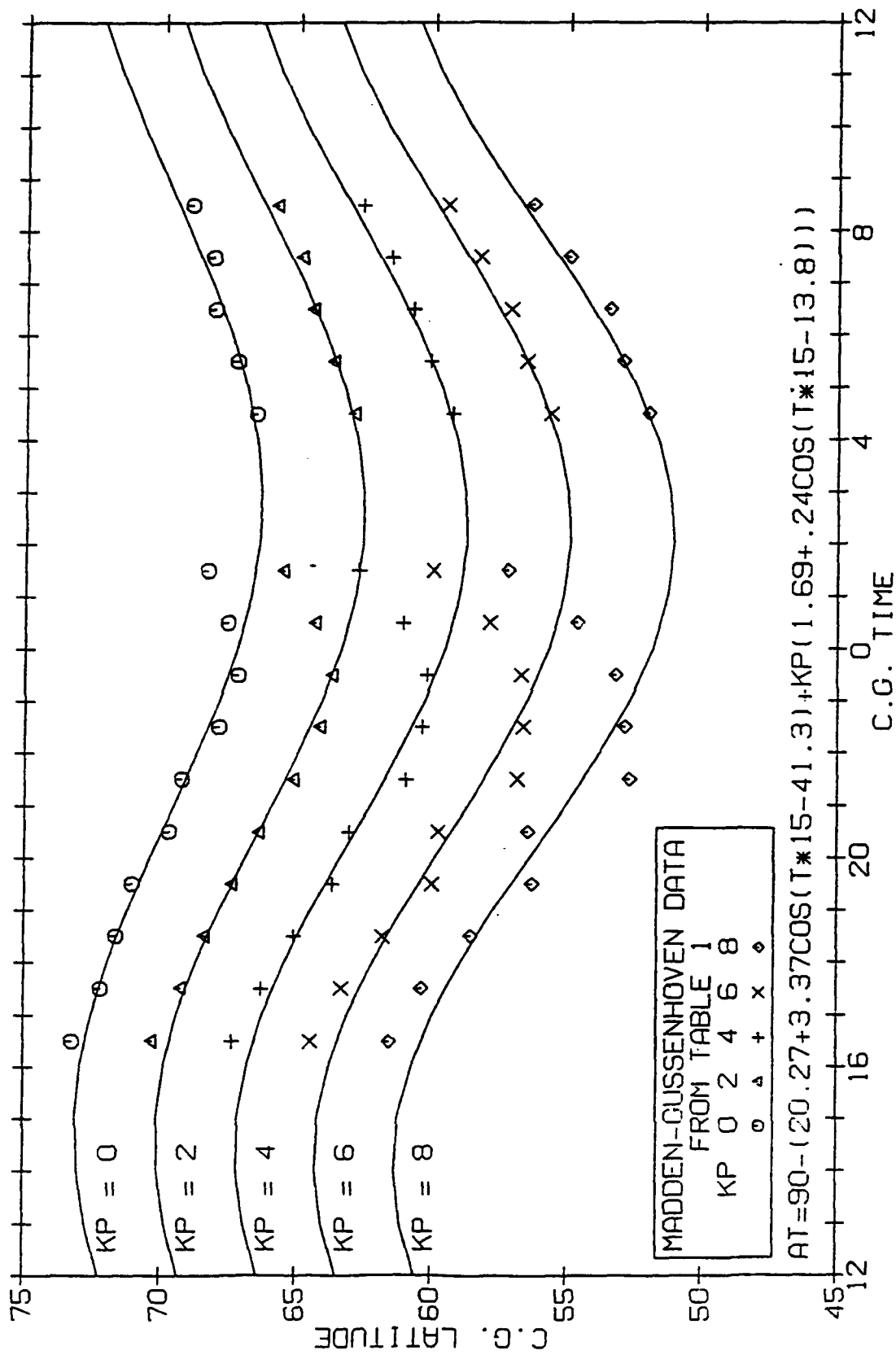


Figure 2. Least Squared Deviation Circle fit to Madden-Gussenhoven Data (Equation 6)

systematic deviation of 00-01-02 hours' data from the experimental fit is not known.

In the following we compare the Q optical auroral ovals with the K_p particle precipitation ovals (using Eq. (6)) for checking the validity of the K_p - Q relation of Eq. (3).

In addition to Eq. (2), Starkov provides a separate equation¹⁰ for $Q=0$ (For the polar ionospheric model the AFGWC uses the Feldstein-Starkov (1967) oval¹² for $Q=0$ and the Starkov equation (Eq. (2) shown above) for $Q \neq 0$). The equation is

$$\lambda_T = 0. - [(72.5 - 3.4 \cos(15T - 18) + 0.7 \cos(2 \cdot T \cdot 15 - 45))]. \quad (7)$$

Starkov optical auroral ovals, for $Q=0$, from Eqs. (2) and (7) are shown in Figure 3. Note that the two $Q=0$ auroral ovals have the same boundary at 16-18 CGT and 06-07 CGT, and the difference is largest (2.9°) around 00-02 CGT, with the Eq. (2) auroral oval more equatorward than that from Eq. (7), and for 09-10 CGT, the auroral oval from Eq. (7) is 1.2° equatorward of that from Eq. (2). For matching the midnight boundary of the auroral oval of Eq. (2) with that from Eq. (7) we need $Q=-3$. To match noon boundaries we need $Q=1$ for Eq. (2). Thus, there is a significant difference between the $Q=0$ auroral ovals from Eqs. (2) and (7).

The next figure (Figure 4) compares auroral ovals, optical for $Q=0$ (Eq. (3)) and particle precipitation for $K_p=0$ (Eq. (7)). Note that both the auroral ovals match for 20-01 CGT but for 10-12 CGT the DMSP K_p particle precipitation auroral oval is 4.5° equatorward of the optical auroral oval.

Figure 5 shows the optical auroral oval for $Q=9$, with particle precipitation ovals for $K_p=2$ and 4. Note that for $K_p=4$ and $Q=9$ the auroral oval boundaries match at 01-02 CGT, whereas at 10-11 CGT the $Q=9$ boundary is closer to that for $K_p=2$.

Thus, we see that there is no good correlation between the Starkov optical and the particle precipitation auroral ovals, especially in the day sector. Significant differences exist between the optical Q and the particle precipitation K_p ovals, because the DMSP boundaries are from the particle precipitation data with a lower threshold of 500 eV that is, with higher sensitivity, than those for the optical emission boundaries for the Feldstein-Starkov auroral ovals determined from the All Sky Camera Systems (ASCA), which had lower sensitivity because of its higher threshold of 1-2 keV. Whalen et al. (1971) observed 6300 Å soft particle precipitation equatorwards of the auroral E layer in the noon sector.¹³ Winningham and Heikkila (1974) characterize these regions as polar rain, polar showers, and polar squalls.¹⁴ The polar showers occur during magnetically quiet conditions whereas the polar squalls occur during magnetically disturbed conditions and are associated with discrete aurora in the night sector. Newell and Meng (1992) show that the polar rain consists of low energy electrons of a few hundred eV associated with the low latitude boundary layer (LLBL), whereas the boundary plasma sheet (BPS) is associated with discrete aurora and the central plasma layer (CPL) is associated with diffuse aurora on the nightside.¹⁵ Thus, in the day sector the precipitation has multiple sources depending on the energy spectrum

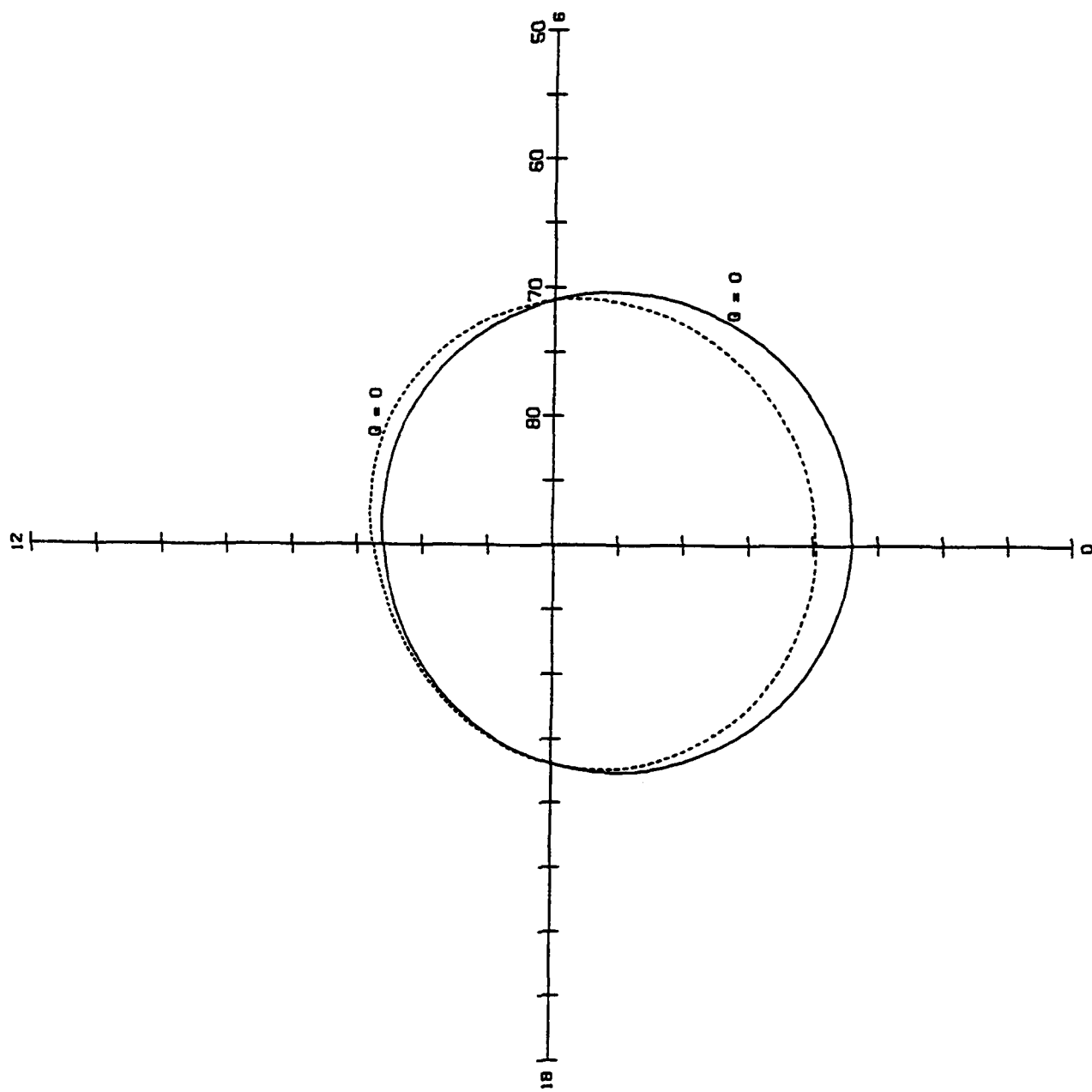


Figure 3. Comparison of Starkov Equations (2 and 7)

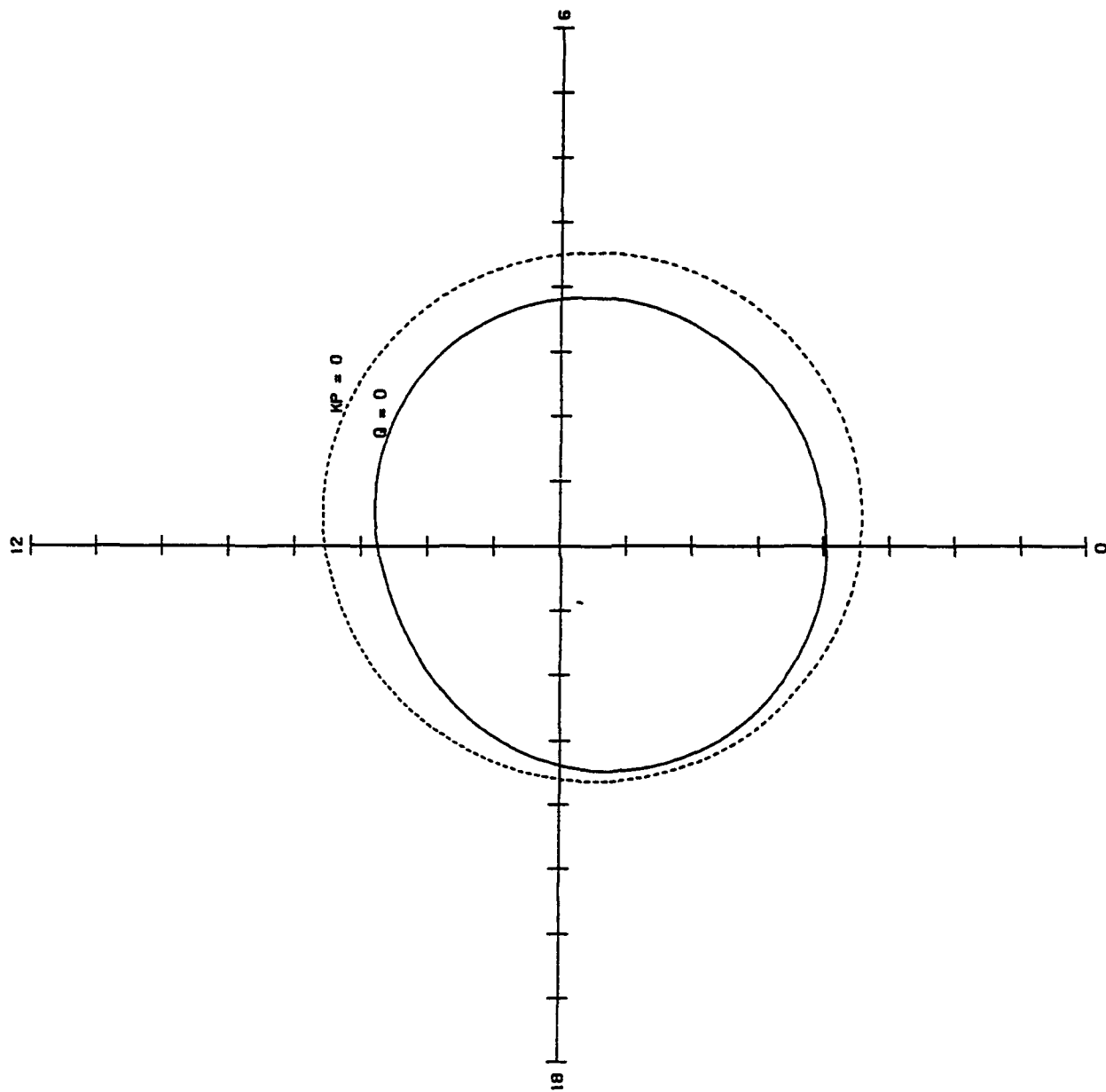


Figure 4. Comparison of Particle Precipitation Oval for $K_p=0$ With Starkov $Q=0$

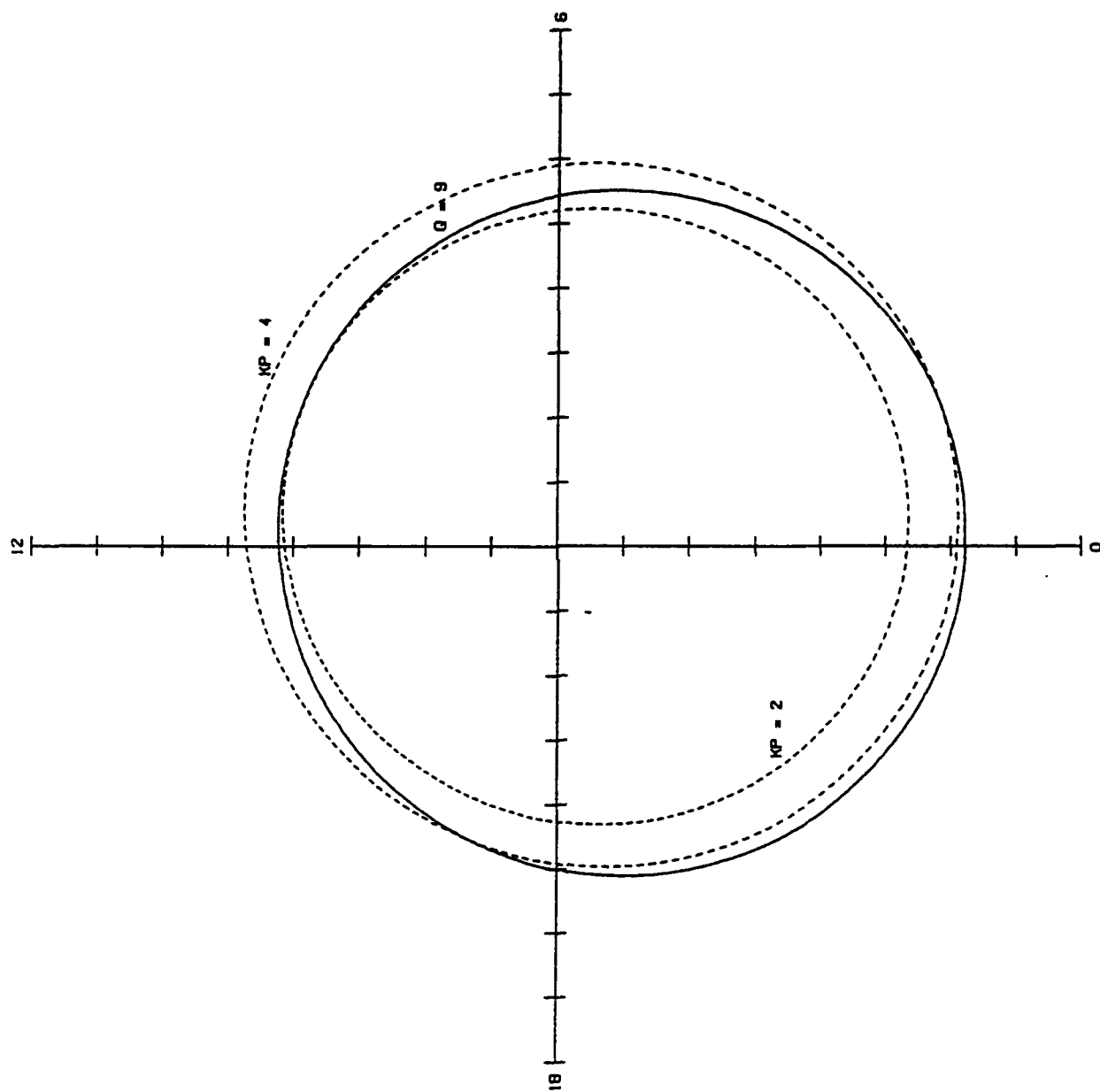


Figure 5. Comparison of Starkov Oval for $Q=9$ With Particle Precipitation Ovals for $Kp=2$ and 4

of the precipitating particles. For the auroral clutter one is more interested in the ionospheric irregularities associated with the auroral E-layer which is the continuous/diffuse auroral oval with a threshold of $\Rightarrow 1$ keV.

In Figure 6 we reproduce Figure (12-12) from the Handbook of Geophysics and the Space Environment¹⁶ to emphasize the difference in thresholds of the respective instruments. Figure 6 shows the magnetic midnight dependence of the equatorward boundary with Kp for electrons (DMSP), auroral oval ASCA photographs, auroral oval from DMSP optical images, and the 6300 Å photometer observations. The excellent match between DMSP electrons and OI 6300 Å emission shows that the DMSP electron sensors with lower thresholds are capable of measuring soft particle precipitation which produces 6300 Å emission at F-layer altitude. The DMSP optical feature: the equatorward boundary of the continuous/diffuse aurora, (usually observed aboard the same satellite measuring the particle precipitation) is collocated with the particle precipitation boundary at very low Kp, and their separation increases with the increase in magnetic activity. In Figure 6, the electrons, the OI 6300 Å emission, and the DMSP optical auroral boundary show very good but different dependencies on Kp. Comparatively, the ASCA observations with relatively poor resolution show more variation for the Q dependence on Kp. For systems operating at high latitudes, the feature of interest is the optical/diffuse/continuous aurora, which originates at E-layer altitudes. The ionospheric irregularities associated with the auroral E layer are the source of auroral clutter, which deteriorates the radar performance at high latitude regions.

The least squared deviation fit to the DMSP diffuse aurora on the midnight meridian in Figure 6 yields the empirical equation

$$\lambda_T = 68.01 - 1.32 * Kp \quad (8)$$

Dandekar¹⁹ derived the empirical fit between the diffuse oval and Kp

$$\lambda_T = 90 - (18.76 + 1.39 * KP + 2.68 \cos(T * 15 - 18)) \quad (9)$$

The corresponding equation with respect to Q is

$$\lambda_T = 90 - (20.85 + 1.01 + 2.55 \cos(15T - 9)) \quad (10)$$

Equations (8) and (9) are in excellent agreement with each other. Comparison of Eqs. (6) and (9) shows that the radius of the particle oval is 23.6° and the rate of increase with Kp is 1.9°,

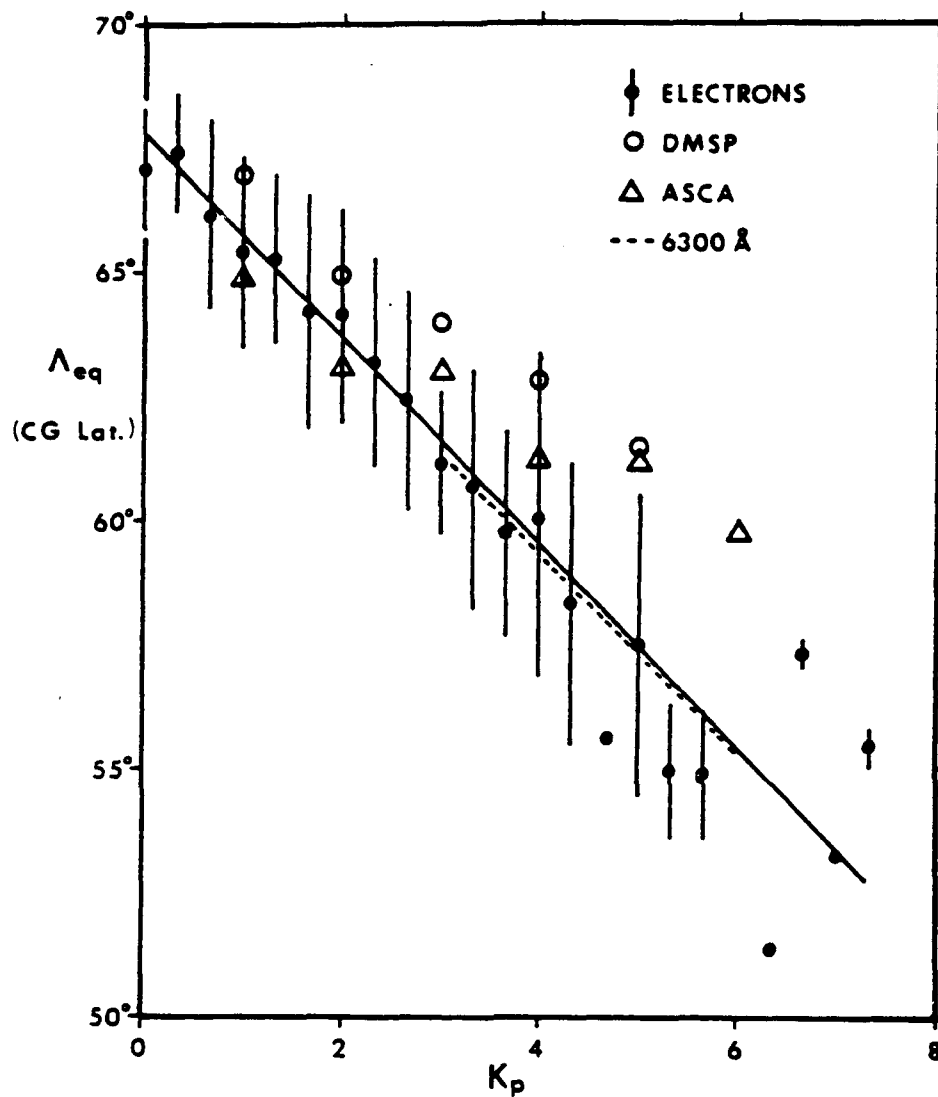


Figure 12-12. Examples of auroral equatorward boundaries near midnight. Electrons: Precipitating electrons [Gussenhoven et al., 1983]⁹ ASCA: All-sky camera photographs [Feldstein and Starkov, 1967]¹² DMSP: DMSP images [Sheehan and Carovillano, 1978]¹⁷ 6300 Å: Photometer [Slater et al., 1980]¹⁸. Error bars indicate standard deviations for the precipitating electrons but are also comparable for the other measurements.

Figure 6. Auroral Equatorward Boundaries Near Midnight for Electrons, DMSP Aurora, ASCA Aurora, and 6300 Å Photometric Observations

whereas the corresponding quantities for the diffuse auroral oval are 21.4° and 1.4° respectively. Thus, the particle precipitation oval is 2.2° larger in radius and expands at a rate that is 0.5° per unit K_p larger than that for the diffuse auroral oval. The Starkov auroral ovals being determined from all sky camera systems (ASCA) are closer to DMSP optical features than to particle precipitation features.

Equations (6) and (7) assume that the center of these ovals is fixed and the radius is a function of the level of magnetic activity. The circles fit to individual Feldstein-Starkov²⁰ auroral ovals (Holzworth and Meng, 1975) show that along with the increase of the radius of the oval, the center of the oval moves away from the CG pole with increasing magnetic activity.²¹ Thus, use of Eqs. (6) and (7) for determination of the K_p - Q relation will result in inaccurate Q values.

3. ANALYSIS

Because of the above background, other possibilities for determining the K_p - Q relations were investigated. The two possible methods for such a determination are 1) a direct use of the observed K_p and Q indices and 2) K_p - and Q -dependent auroral oval features like various oval boundaries, determined from the observed common data sets.

The planetary K_p index is not available in real time to support the active operating systems. Therefore, the AWS generates its own AWS-K index, which is similar to the K_p index. At present the Q index is available from a single station, Sodankyla. This index is not available to AWS in real time. Moreover, Dandekar (1979) showed that the Q index measured from a single station is not accurate at all times because the station cyclically moves closer and away from the auroral oval due to the diurnal rotation of the earth.¹⁹ The Q data are reliable only when the station is near the auroral oval around magnetic midnight. Dandekar (1982) studied March 1978-May 1981 Q and K_p and AWS-K data,⁵ for determining hourly dependence between Q , AWS-K and K_p . The results are presented in Table 3, row 1 for 01-02 UT when the station Sodankyla is on the magnetic midnight meridian. The rate of increase of Q is 1.4 times that of K_p and not twice K_p as given in Eq. (3).

Using the larger data base of the remaining 22 hours, Dandekar used the correction factors¹⁹ for correcting and detrending the Q index data. The cumulative distributions of the corrected (detrended) Q data and the corresponding K_p data for the four years are shown in Figures 7A and 7B. The figures show that the distributions of both K_p and Q indices were very similar in years 1969 (close to the maximum of the sunspot cycle 20) and 1971 (approximate midpoint of the descending part of sunspot cycle 20). The distributions in 1965 (closer to sunspot minimum of sunspot cycles 19-20) and 1974 (towards the minimum of the later part of sunspot cycle 20) show the largest differences. The data for these years were selected to represent a complete solar cycle. From Figures 7A and 7B, the corresponding values of K_p - Q indices were computed at every 5 percent interval of the population. These K_p - Q values for the four years are shown in Figure 8. The least squared deviation straight line fit for all the data of each year are shown in row 2 of Table 3. On the average, Q increases at the rate of $1.56 \cdot K_p$ and not at twice K_p as given in Eq. (3). The table shows that the results from detrended Q data are in good agreement with those

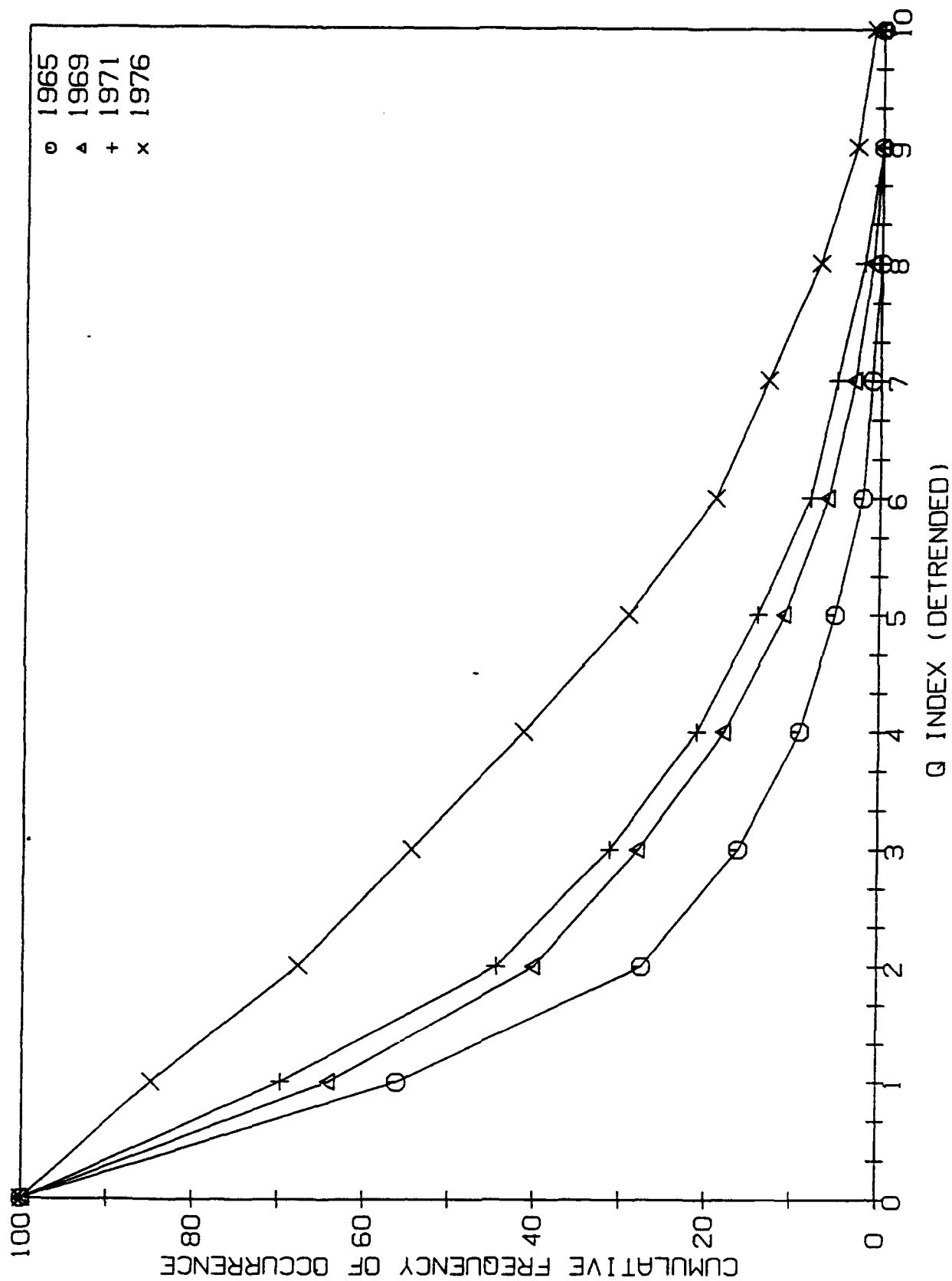


Figure 7A. Cumulative Population of Detrended Q Index for Years 1965, 1969, 1971, and 1974

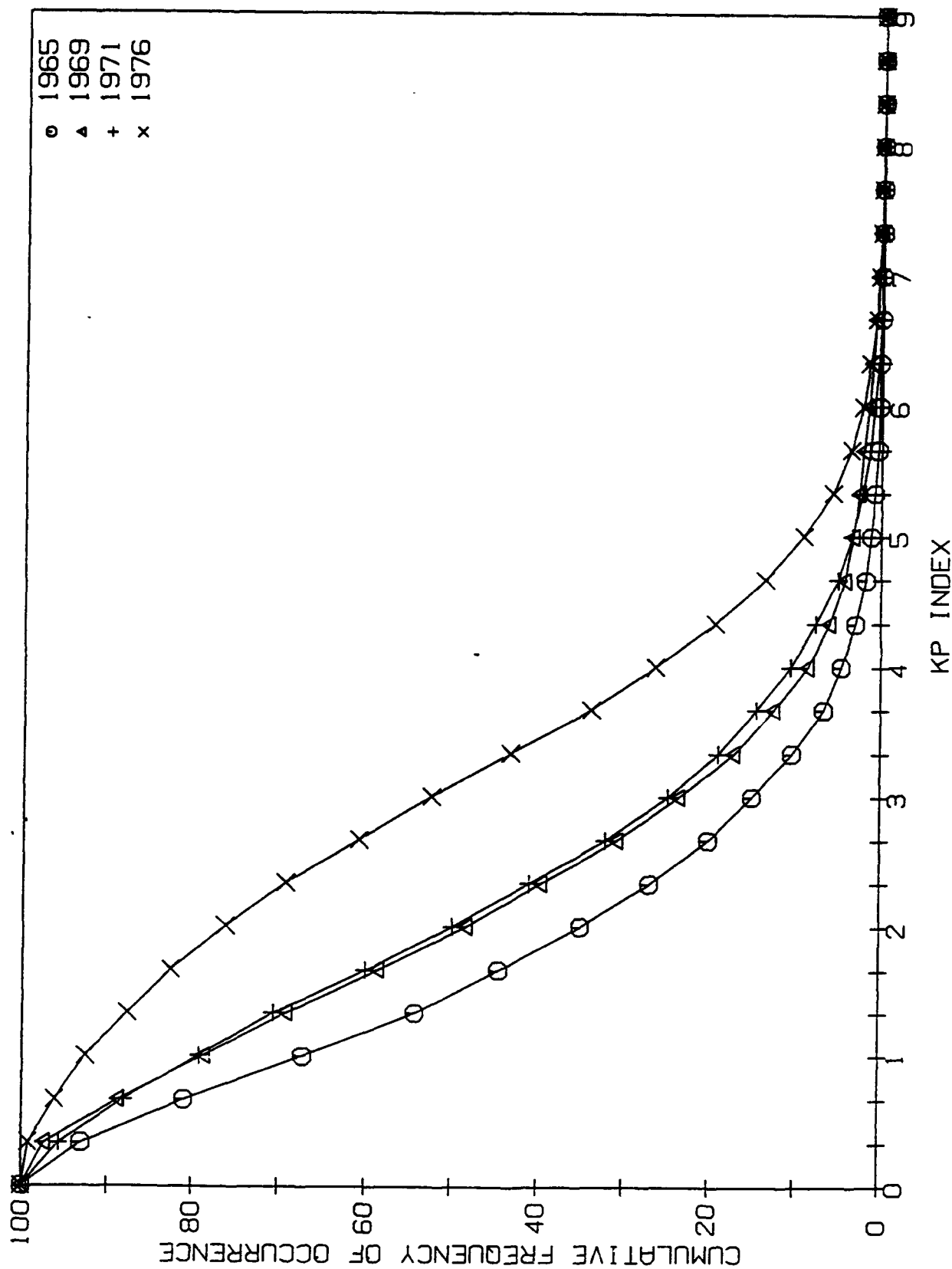


Figure 7B. Cumulative Population of Kp Index for Years 1965, 1969, 1971, and 1974

restricted to the midnight meridian situations (first two blocks of Table 3).

The preliminary study had shown that the data should be divided into two intervals: 1) $K_p \leq 2+$ and 2) $K_p > 2+$. The results of the least squared deviation straight line fits for these two cases are presented in rows 3 and 4 of Table 3 and in Figure 8. When the data are divided into two intervals of K_p , the K_p - Q dependence in these two intervals is significantly different (blocks 3 & 4 of Table 3). One can use either set (a single range or two K_p intervals). The comparison of these results with Hardy Eq. (3) shows that for high K_p ($>2+$) values the slopes are in good agreement, but for low K_p ($\leq 2+$) values the slope is about half of that of the Hardy equation. The cutoff from Hardy matches with that for low K_p , but for high K_p the difference is quite significant. Thus, in general the Hardy equation does overestimate the Q values.

The equatorward auroral oval boundaries for the midnight meridian computed from the Hardy equation are available from the CRRES program.¹¹ The K_p indices computed from these boundaries are shown with the planetary K_p indices for 7687 observations over a six-month period (July-December 1990) in Figure 9. The middle curve shows the median whereas the lower and upper curves show the respective $\pm \sigma$ levels. Up to $K_p \leq 3$ both the indices are in good agreement. The $K_p > 3$ determined from CRRES observations is slightly overestimated with increasing K_p . Thus, particle precipitation ovals provide really good estimates of K_p . It is the K_p - Q relation in Eq. (3) which looks inaccurate.

The small sample of AWS-K data (in Figure 2) is compared with the K_p data in Figure 10. The figure shows that the AWS-K is overestimated with respect to K_p for $K_p < 3$. The over-estimation of AWS-K would also result in overestimation of Q from the Hardy Eq. (3). It is essential to look at a larger AWS-K data base to see if the over estimation of K_p in the lower ranges is a persistent problem.

Now let us look at the indirect determination of the K_p - Q relation. Feldstein and Starkov determined the dependence of the three (poleward, middle, and equatorward) optical auroral oval boundaries from the all sky camera systems (ASCA) with respect to Q and K_p indices.¹² The fit to the equatorward boundary of the Feldstein-Starkov data (Figure 2D, 1967) yields

$$\lambda = 68.93 - 1.37 Q \quad (11)$$

This equation is in good agreement with that for the diffuse aurora observed aboard DMSP satellites, shown in Figure 6 and in Eq. (8) given above.

Feldstein and Starkov graphically presented various auroral oval boundaries¹² as functions of the K_p and Q indices. These data are read from the graphs. The detrended Q and K_p populations¹⁹ are used as weighting factors in determining least squared deviation straight line fits to the respective data (the data points showing large deviations from the straight line fit were not used). The respective relations tying latitude location to K_p/Q were used for determining the K_p - Q relationships. These are presented in Table 4.

Dandekar determined empirical relations¹⁹ between the level of magnetic activity (K_p and Q

Table 2. Parameters of the Starkov Q and Hardy Kp Ovals
(COMPARISON OF STARKOV (EQ2) AND HARDY (EQ6) OVALS)

OVAL	RADIUS	OFFSET FROM CG POLE	CHANGE IN RADIUS
STARKOV-Q	$(18+5.1)=23.1$	5.1	.9 PER UNIT Q
HARDY-KP	$(20.27+3.37)=23.6$	3.4	1.7 PER UNIT KP

Table 3. Kp-Q Relation From Observed Kp-Q Data

EQUATION FOR Q-KP	SOURCE	REFERENCE
$Q=1.314K+0.911$	FIGS 2A & 2B ²²	GEOMAG & AERONOMY ENG.ED. 7, 1967, P49
$Q=1.165K+1.273$	FIGS 3A & 3C ²² EQUATORWARD NIGHT BOUNDARY	GEOMAG & AERONOMY ENG.ED. 7, 1967, P50
$Q=1.030K+3.245$	FIGS 3A & 3C ²² POLEWARD NIGHT BOUNDARY	GEOMAG & AERONOMY ENG.ED. 7, 1967, P50
$Q=1.716K-4.413$	FIGS 4A & 4C ²² POLEWARD DAY BOUNDARY	GEOMAG & AERONOMY ENG.ED. 7, 1967, P50
$Q=2.167K-2.058$	FIGS 4A & 4C ²² EQUATORWARD DAY BOUNDARY	GEOMAG & AERONOMY ENG.ED. 7, 1967, P50
$Q=1.506K+0.625$	FIGS 5 OVAL WIDTH	GEOMAG & AERONOMY ENG.ED. 7, 1967, P51
$Q=1.376K-1.9$ $Q=1.333K-2.0$	N. HEMISPHERE DMSP DATA ⁶ S. HEMISPHERE DMSP DATA ⁶	AFGL-TR- 79-0010

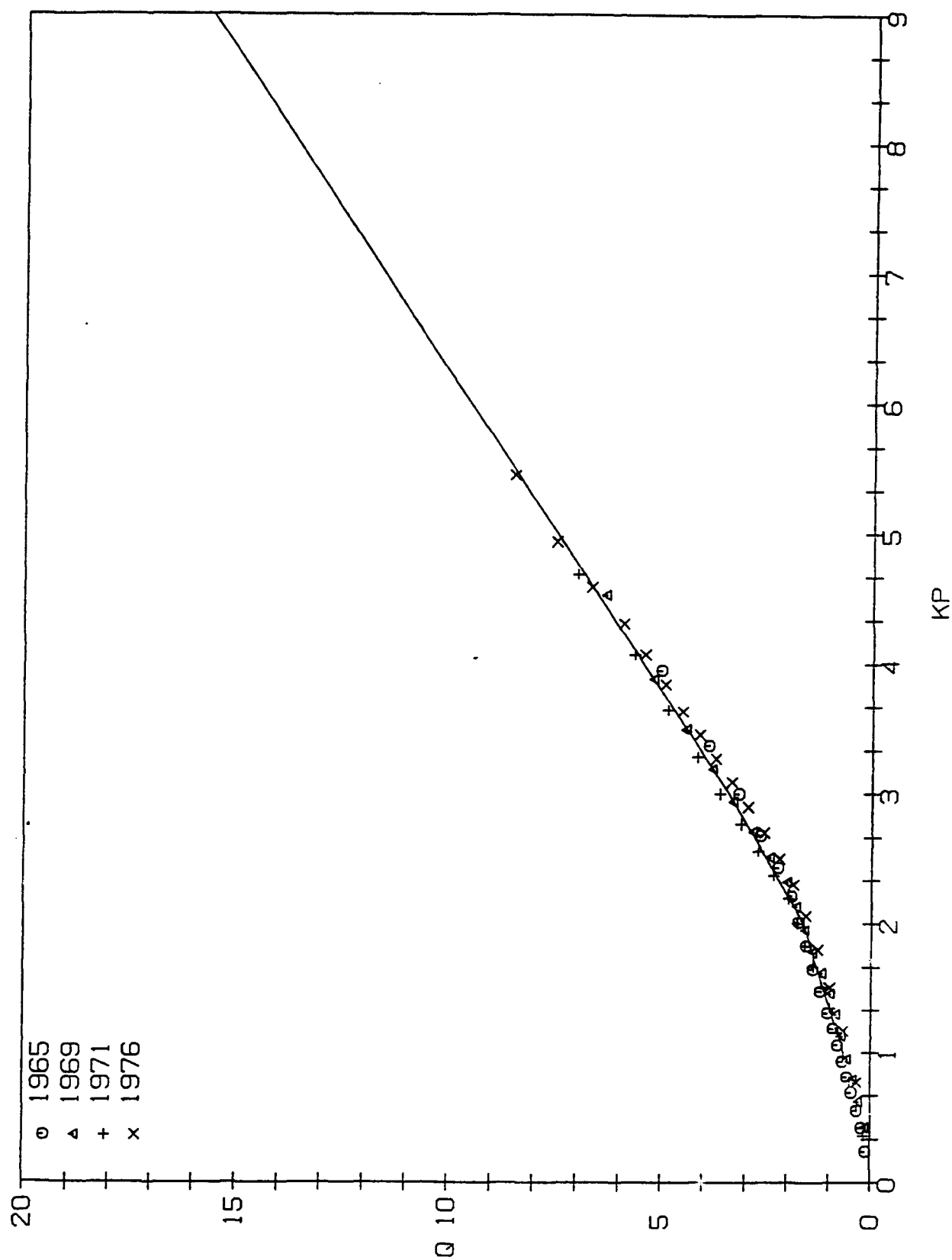


Figure 8. Relation Between the Kp and the Q Index From the Four-Year Data

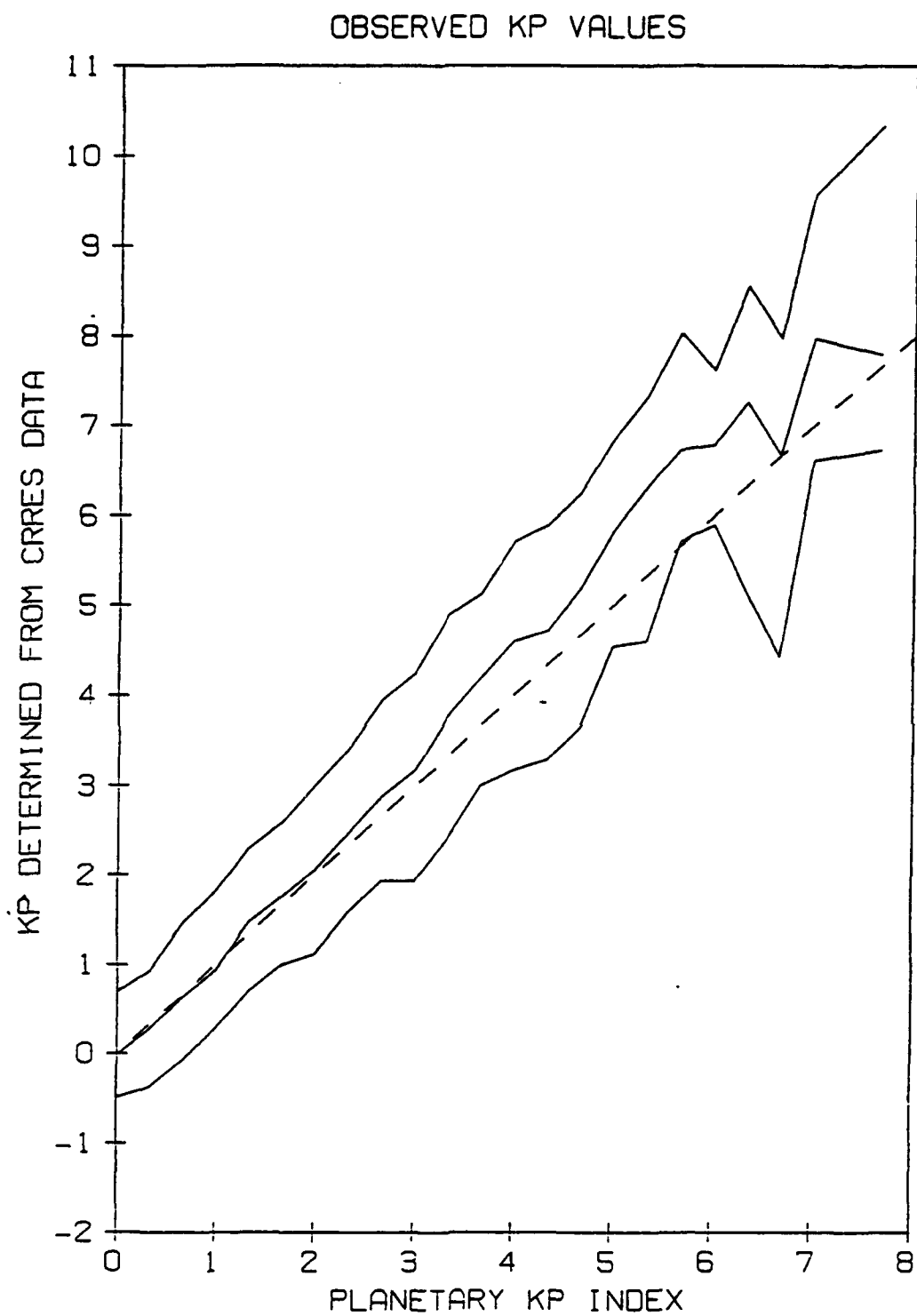


Figure 9. Comparison of Auroral Kp Index With the Planetary Kp Index From CRRES Data of July-December 1990

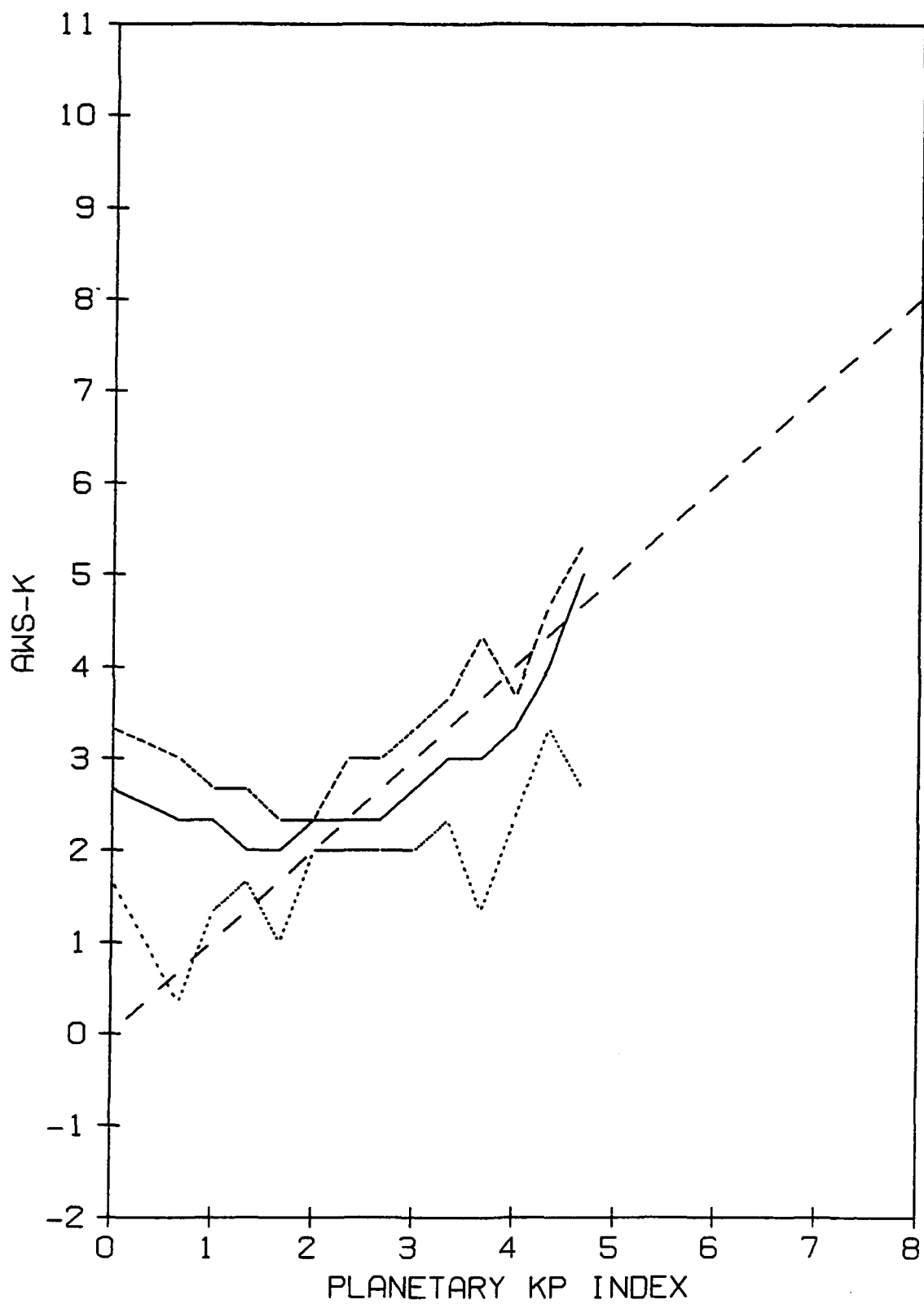


Figure 10. Comparison of the AWS -K Index With the Planetary Kp Index

Table 4. Kp-Q Relation From Oval Parameters

EQUATION	REFERENCE	REMARKS
$Q=1.37 * KP^{-1.7}$ (01.02 UT)	DANDEKAR(1982) ⁵ AFGL-TR-82-0010	SODANKYLA, FINLAND 67.4 N, 26.6 E
$Q=1.245 * KP^{-0.5}$ $Q=1.519 * KP^{-1.1}$ $Q=1.581 * KP^{-1.0}$ $Q=1.823 * KP^{-2.0}$ $Q=1.558 * KP^{-1.1}$	PRESENT STUDY	1965 1969 1971 1974 ALL FOUR YEARS
$Q=0.962 * KP^{-0.2}$ $Q=0.989 * KP^{-0.4}$ $Q=1.007 * KP^{-0.3}$ $Q=1.065 * KP^{-0.6}$ $Q=0.964 * KP^{-0.3}$	PRESENT STUDY	1965 1969 1971 1974 ALL FOUR YEARS FOR $KP \leq 2+$
$Q=1.871 * KP^{-2.4}$ $Q=1.950 * KP^{-2.4}$ $Q=2.000 * KP^{-2.4}$ $Q=2.189 * KP^{-3.4}$ $Q=2.040 * KP^{-2.7}$	PRESENT STUDY	1965 1969 1971 1974 ALL FOUR YEARS FOR $KP > 2+$
$Q=1.125 * KP^{-0.7}$ $Q=1.497 * KP^{-1.0}$ $Q=1.302 * KP^{-0.7}$ $Q=1.545 * KP^{-1.4}$ $Q=1.367 * KP^{-0.9}$	DANDEKAR(1982) ⁵ AFGL-TR-82-0010 (ADA118734)	1965 1969 1971 1974 ALL FOUR YEARS

(not detrended)) and the equatorward boundary of the optical continuous/diffuse of both northern and southern hemispheric aurora observed aboard the DMSP satellites. The results are shown in Table 4.

Thus, in general, results in Table 4 show that Q increases approximately at the rate of $1.5 \cdot K_p$ and not at twice the rate of K_p as determined by Hardy in Eq. (3).

4. CONCLUSIONS

The particle precipitation auroral ovals do provide a good real time estimate of the K_p index. In the above we see that matching the particle precipitation auroral ovals with the Starkov optical auroral ovals leads to an inaccurate determination of the K_p - Q relationship. It would be nice to have a midnight meridian Q index to compare with the planetary K_p index for determining the K_p - Q relation. However a reasonably direct relationship between K_p and Q is obtained by correcting the observed single station Q data for the diurnal rotation of the earth under the auroral oval. For a better accuracy in the determination of the Q index, the K_p range is divided in two intervals. The improved, more precise Q values obtained from this procedure will improve the prediction of the auroral oval phenomena that affect the performance of the real time operational systems in high latitude regions.

References

1. Barghausen, A.L., Finney, J.W., Proctor, L.L., and Schultz, L.D., (1969) *Predicting Long Term Operational Parameters of High Frequency Sky-Wave Tele-Communication Systems*, ESSA Tech.Rep. ERL 110-ITS78.
2. Lloyd, J.L., Haydon, G.W., Lucas, D.L., and Teters, L.R., (1978) *Estimating the Performance of Telecommunication Systems Using the Ionospheric Transmission Channel*, National Telecommunications and Information Administration, Boulder, Colorado.
3. Millman, G.H., Bowser, C. A., and Swanson R.W., (1988) An Ionospheric Model for HF Sky-wave Backscatter Radar; presented at the NATO-AGARD Symposium on "Ionospheric Structure and Variability on a Global Scale and Interactions with Atmosphere," Munich, Federal Republic of Germany, May 16-20,1988.
4. Prochaska, R.D., Capt., *Geomagnetic Index Calculation and Use at AFGWC*, AFGWV/Tn-80/002.
5. Dandekar B. S.(1982) *The Statistical Relations Among Q, Kp, and the Global Air Weather Central-K Indices*, AFGL-TR-82-0010, ADA084808.
6. Dandekar B. S.(1979) *Study of the Equatorward Edge of the Auroral Oval From Satellite Observations*, AFGL-TR-79-0010, ADA072997.
7. Hardy D. A. (private communication)
8. Gussenhoven, M.S., Hardy, D.A., and Burke, W.J.(1981) DMSP/F2 Electron Observations of Equatorward Auroral Boundaries and Their Relationship to Magnetospheric Electric fields, *J.Geophys. Res.*, **86**(A2):768.
9. Gussenhoven, M.S., Hardy, D.A., and Heinemann, N., (1983), Systematics of the Equatorward Diffuse Auroral Boundary, *J.Geophys. Res.*, **88**(A7):5692-5708.
10. Starkov, G. V.(1969) Analytical representation of the equatorial boundary of the oval auroral zone, *Geomagn. Aeron.* (Eng. ed.) **9**:614.
11. Madden, D. and Gussenhoven, M. S.(1990) *Auroral Boundary Index From 1983 to 1990*, GL-TR-90-0358, ADA232845.
12. Feldstein, Y. I., and Starkov, G.V. (1967), Dynamics of Auroral Belt and Polar Geomagnetic Disturbances, *Planet. Space Sci.* **15**:209.
13. Whalen, J.A., Buchau, J., Wagner, R.A. (1971) Airborne ionospheric and optical measurements of noontime aurora, *J. Atmos. Terr. Phys.*, **33**:661.
14. Winningham, J.D., and Heikkila, W.J., (1974) Polar Cap Auroral Electron Fluxes Observed With Isis 1, *J. Geophys. Res.*, **79**(7):949-957.

15. Newell, P.T., and Meng, C.I., (1992) Mapping the Dayside Ionosphere to the Magnetosphere According to Particle Precipitation Characteristics, *JGR Letters*, 19(6):609-612.
16. Jursa A. S., scientific editor, (1985) *Handbook of Geophysics and the Space Environment*, Air Force Geophysics Laboratory, Air Force Systems Command, USAF, AFGL-TR-85-0315, ADA167000.
17. Sheehan, R. E., and Carovillano, R. L.(1978) Characteristics of the equatorward auroral boundary near midnight determined from DMSP images, *J. Geophys. Res.*, 83(A10):4749.
18. Slater, D. W., Smith, L. L., and Kleckner, E. W. (1980), Correlated Observations of the Equatorward Diffuse Auroral boundary, *J. Geophys. Res.*, 85:531.
19. Dandekar, B. S.(1979) *Magnetic Disturbance Statistics From a Single Station Q Index Applied to an Actual OTH-B Radar Situation*, AFGL-TR-79-0296, ADA084808.
20. Feldstein, Y. I., and Starkov, G. V.(1970) The auroral oval and the boundary of closed field lines of geomagnetic field, *Planet. Space Sci.* 18:501.
21. Holzworth, R. H., and Meng, C.-I.(1975), Mathematical representation of the auroral oval., *Geophys. Res. Lett.*, 2:377-380.
22. Starkov, G. V., and Feldstein, Y. I.(1967), Change in the boundaries of the oval auroral zone, *Geomagn. Aeron.* (Eng. ed) 7:48.